The impact of historical land use/land cover change on regional climate extremes

Kirsten L. Findell[1], Alexis Berg[2], Pierre Gentine[3], John P. Krasting[1], Benjamin R. Lintner[4], Sergey Malyshev[1], Joseph A. Santanello Jr.[5], Elena Shevliakova[1]*

For submission to Nature Communications

[1]Geophysical Fluid Dynamics Laboratory, Princeton, NJ
[2]Princeton University, Dept. of Civil and Environmental Engineering
[3]Columbia University, Dept. of Earth and Environmental Engineering
[4]Rutgers University, Dept. of Environmental Sciences
[5]NASA GSFC Hydrological Sciences Branch, Greenbelt, MD
**Corresponding author: Kirsten.Findell@noaa.gov*

Abstract

Recent research highlights the role of land surface processes in heat waves, droughts, and other extreme events. Here we use an earth system model (ESM) from the Geophysical Fluid Dynamics Laboratory (GFDL) to investigate the regional impacts of historical anthropogenic land use/land cover change (LULCC) on combined extremes of temperature and humidity. A bivariate assessment allows us to consider aridity and moist enthalpy extremes, quantities central to human experience of near-surface climate conditions. We show that according to this model, conversion of forests to cropland has contributed to much of the upper central US and central Europe experiencing extreme hot, dry summers every 2-3 years instead of every 10 years. In the tropics, historical patterns of wood harvesting, shifting cultivation and regrowth of secondary vegetation have enhanced near surface moist enthalpy, leading to extensive increases in the occurrence of humid conditions throughout the tropics year round. These critical land use processes and practices are not included in many current generation land models, yet these results identify them as critical factors in the energy and water cycles of the midlatitudes and tropics.

1 Motivation

The catastrophic summertime heat wave events in Western Europe in 2003 and Russia in 2010 inspired much new research on extreme events (e.g., Fischer and Schar, 2010; Stott et al., 2004). Vegetation and surface moisture conditions have been shown to impact both the severity and duration of heat wave events (e.g., Miralles et al., 2014; Stefanon et al., 2012; Davin et al., 2014;

Lemordant et al., 2016), as well as the aridity over land in the future (Berg et al., 2016). In particular, plant water use strategies (from more intensive water user to more conservative) can drastically impact heat wave severity (Teuling et al. 2010; van Heerwaarden and Teuling 2014).

Previous model-based studies of the impact of historical land use/land cover change (LULCC) on temperature extremes have produced contrasting results. Christidis et al. (2013) show that extremes are less severe with deforestation, while Strack et al. (2008) show enhanced severity, and the model intercomparison of Pitman et al. (2012) shows model responses of opposing signs. This spread of model response in extreme temperatures is consistent with the more extensive literature related to the mean temperature response to LULCC. In the temperate mid-latitudes there is uncertainty about the relative importance of competing biophysical influences (Pitman et al., 2009; De Noblet-Ducoudre et al., 2012), with some models showing that the albedo-driven warming effect of forest cover is dominant (e.g., Bonan 1999, Oleson et al., 2004), and others showing that deeper roots and higher turbulent exchange of forests yield cooler conditions than pastures or crops (e.g., Findell et al. 2007, 2009; Jackson et al, 2005; Malyshev et al., 2015). Recent work has demonstrated that surface roughness differences are the dominant factor in the Amazon (Khanna and Medvigy, 2014) and in the northern mid-latitudes (Chen and Dirmeyer, 2016). Despite these differences in the annual mean signal, the models do show agreement on the seasonality of these influences, with the albedo effects strongest in winter and the flux-related influences strongest in summer.

Some observational evidence exists for a latitudinal dependence in the balance between the cooling and warming factors influencing the response to deforestation (Lee et al., 2011). Satellite-based observational studies show that mid-latitude forests are cooler than nearby cleared lands in the daily mean and maximum air temperature, particularly in summer but also in the annual mean (Alkama and Cescatti, 2016; Li et al., 2015), and that mid-latitude forests throughout the US are cooler than nearby cleared lands from spring through fall, and in all seasons in the southeastern US (Wickham et al., 2012).

Given the importance of vegetation and soil moisture in regulating surface fluxes of heat and moisture, we consider the impact of anthropogenic LULCC on regional climate extremes using a novel approach to characterize the joint temperature–humidity response to historical LULCC. Most previous studies of LULCC impacts have focused on single-variable assessments typically involving temperature and precipitation (e.g., Findell et al., 2007, 2009; Pitman et al., 2009). However, quantities relevant to human capacity to cope with or adapt to climatic conditions typically consider both the temperature and humidity of near-surface air (e.g., Sherwood and Huber, 2010; Knutson and Ploshay, 2016; Pal and Eltahir, 2016). Furthermore, plant physiological stress and ecosystem health is heavily impacted by the vapor pressure deficit of near-surface air. Including both humidity and temperature in this analysis allows us to consider aridity and moist enthalpy: quantities that are closely related to vapor pressure deficit and wet bulb temperature, respectively, and are central to ecosystem health and human perception and experience of near-surface climate conditions (Sherwood and Huber, 2010).

Using the GFDL ESM described in Section 2, we compare the historical (i.e. 1860-2005) all-forcing simulation (AllHist) from the GFDL submission to the Coupled Model Intercomparison Project (CMIP5, Taylor et al., 2012) to a simulation in which the historical land use reconstruction (Hurtt et al., 2011) is replaced with potential vegetation at all time steps (PotVeg; the vegetation that would be present at each grid cell with no human interference in the landscape). This ESM is at the forefront of process-inclusion, particularly with regard to land use processes in the tropics such as wood harvesting, shifting cultivation, and secondary vegetation growth (Houghton et al., 2012). Furthermore, its deforestation responses have been found to be well within available observational constraints (e.g., Alkama and Cescatti, 2016; Li et al., 2015; Wickham et al., 2012). These factors provide important rationale for our analysis, though we acknowledge the limitations of a single model in terms of generalizability. We note, however, that the analysis protocol introduced here can be applied to output from the suite of models participating in the upcoming Land Use Model Intercomparison Project (LUMIP; Lawrence et al., 2016). Results from the experiments outlined in Section 2 are discussed in Section 3, first for the northern mid-latitudes and then for the tropics. Conclusions are presented in Section 4.

2 Methods

2.1 Model and Experiments

Data analyzed are from two sets of simulations of the GFDL ESM2G model (Dunne et al. 2012, 2013), which includes the terrestrial component LM3.0, representing both vegetation dynamics (Shevliakova et al., 2009) and land hydrology (Milly et al., 2014). The atmosphere and land components' resolution is 2˚ latitude by 2.5˚ longitude, with 24 vertical levels in the atmosphere and 20 layers in the soil. LM3.0 simulates changes in vegetation and soil carbon pools, effects of LULCC on them, as well as exchanges of water, energy, and carbon between the land and the atmosphere. Vegetation is represented by one of five types: deciduous, coniferous, and tropical trees, as well as cold and warm grasses. Subgrid land-use heterogeneity is resolved through the use of up to 15 different tiles with differing land-use histories, separately tracking above- and below-ground differences in hydrological and carbon states of croplands, pastures, natural, and secondary lands. Vegetation height, leaf area index (LAI), and the seasonality of leaf cover are determined prognostically in each vegetation tile.

The decadal-average land-use history is prescribed from the Hurtt et al. (2011) reconstruction for each grid cell in terms of transition rates between four different land-use types: natural (i.e. undisturbed by humans), croplands, pastures, and secondary lands (i.e. previously logged or abandoned). The transition-based approach used in LM3.0 creates more land-cover disturbance than the fraction-based approach (Shevliakova et al., 2013) because the transitions reflect the paths of changes among different use categories—and thus the "gross transitions"—between different land-use types, rather than just the net effect based on changes in fractions. These gross

sub-grid changes include shifting cultivation and secondary-to-secondary transitions representing wood harvesting of secondary forests.

Land-use transitions are applied annually at the end of the calendar year based on interpolation between the decadal averages. Each grid cell can have up to 10 secondary tiles to capture age and thus biomass distribution. In each grid cell secondary tiles with similar vegetation biomass are merged for computational efficiency. Harvesting of crops and pastures is applied annually, though with differing intensities: all but 0.1 kg C m^{-2} of crop biomass is removed annually, while on pastures, 25% of leaf biomass is removed each year (Shevliakova et al., 2009). Some grid cells also include lakes and/or glacier tiles.

On vegetated tiles evapotranspiration (ET) in LM3.0 can occur through three pathways: from soil and/or snow surface evaporation, plant interception, and through transpiration. Transpiration is a function of plant stomatal conductance and soil water availability, which depends on the vertical distribution of plant roots and soil moisture in each land-use tile (Milly et al., 2014). An important feature of LM3.0 is that each land-use tile has its own soil water and plant root distribution: thus, evapotranspiration is not a function of the grid-cell average soil moisture.

Here, we compare the historical (i.e. 1860-2005) all-forcing simulation (AllHist) with simulations that do not include any anthropogenic interference through LULCC, referred to as the potential vegetation (PotVeg) experiment. All other radiative forcings in PotVeg are identical to those in the AllHist experiment. In both runs, the atmospheric CO_2 seen by the model's radiation code was restored to the observed historical trend on a 1 year time scale. Two ensemble members of each experiment were analyzed, with the last 25 years of each ensemble member (1981-2005) included in our analysis. Figure 1a shows the spatial coverage of natural species depicted in the PotVeg run during this time period, while Figures 1b-e show the average fraction of the four land-use types at the end of the AllHist experiment. Secondary vegetation is prominent throughout Europe, along the southern border of the cold evergreen forests of Eurasia, in the Eastern United States, around the margins of Amazonia, and in large sections of northern and central Africa. National boundaries are clearly evident in the natural and secondary characterizations of northern Africa as a result of using national wood harvest statistics as an input to the Hurtt et al. (2011) reconstruction.

Croplands are prominent in the upper Midwestern US and extending into the central provinces of Canada, in India, and throughout Europe, particularly eastern Europe. There are more modest percentages of croplands in Central America, the eastern part of West Africa, and in southeastern China. Pastures are dominant in the central US, throughout central Asia, the Sahel, southern Africa, southeastern South America, and Australia.

2.2 Analysis methods

Statistical significance is determined through the use of two-tailed t-tests at the 90% significance level for Figure 2, and the more stringent modified two-tailed t-test for Figure 3, also at the 90%

significance level. The modified t-test accounts for autocorrelation within the time series (von Storch and Zwiers, 1999; Findell et al., 2006).

We use mixing diagrams following Betts (1992) and Santanello et al. (2009) to show changes in the climatology and diurnal cycles induced by LULLC. The conserved variable diagrams of Figure 4 depict, in common units of kJ/kg, λq on the x-axis and c_pT on the y-axis, where λ is the latent heat of condensation, c_p is the specific heat of dry air at constant pressure and q and T are 2m humidity and temperature. To quantify the occurrence of hot, dry extremes, we wish to compare how the data from each experiment occupy the upper left portion of the mixing diagrams in Figure 4. We define another set of orthogonal axes using the moist enthalpy, ME = $\lambda q + c_pT$, and lines orthogonal to ME. ME is a measure of the total internal energy of moist air, and is largest in the upper right portion of the mixing diagrams. We use lines orthogonal to constant ME lines as a proxy for aridity, with aridity largest in the upper left corner of the mixing diagrams. We calculate the 10^{th} and 90^{th} percentile threshold values for the monthly mean ME and aridity proxy. These threshold values are shown in Figure 4c with solid green (PotVeg) and black (AllHist) lines. Exceedances of these threshold values are calculated at each grid point, and the return periods associated with these exceedance rates are shown in Figures 5a and 5b for individual months, with significance determined using a Wilcoxon rank sum test at the 5% significance level. Seasonal, latitudinal means of these return periods are shown in Figure 5c. Our results do not change appreciably if we use wet-bulb temperature and relative humidity instead of ME and our aridity proxy (compare Figure 5 with Figure S1), though the independence of the two measures is lost.

3 Results

3.1 Northern Mid-latitude response to historical LULCC

The summertime northern mid-latitude response to historical LULCC (Figure 2) is dominated by a reduction of latent heat flux (particularly through transpiration, not shown) and an increase of sensible heat flux, particularly in regions converted to croplands. These areas also show large reductions in LAI and gross primary productivity (GPP). As shown in Figure 3 in combined humidity-temperature phase-space, the changes in vegetation characteristics and functioning are accompanied by a statistically significant mid-latitude warming and drying of the near-surface atmosphere, i.e., the differences pass a modified t-test accounting for autocorrelation within the time series (von Storch and Zwiers, 1999; Findell et al., 2006). These results are consistent with the analysis of temperature fields in Findell et al. (2007, 2009) using earlier generation models at GFDL that showed statistically significant near-surface warming in regions with historical LULCC.

To further understand the midlatitude warming and drying, we use mixing diagrams following Betts (1992) and Santanello et al. (2009) to show changes in the climatology and diurnal cycles induced by LULLC. July monthly mean diurnal cycles (7 am to 6 am) for the 50 years of each

scenario (two ensembles members with 25 simulation years each) are shown in Figures 4a and 4b for a single grid point in Iowa, which is broadly representative of midlatitude croplands. Over the sampled pixel, nighttime values tend to be at or near saturation[1] for the PotVeg diurnal cycles (Figure 4b), while the mid- to late-afternoon values generally have relative humidity (RH) values of 75-85%. The 50 corresponding AllHist July diurnal cycles (Figure 4a) show much warmer and drier conditions, with no instances of afternoon RH values above 80%, and a few years drying past 50% RH in the late afternoon. The mean diurnal cycles for these 50 years (Figure 4c) reflect these changes: anthropogenic LULCC shifts the mean July diurnal cycle in Iowa to warmer, drier conditions, with afternoon RH decreasing from close to 80% in the PotVeg experiment to less than 70% in the AllHist experiment. The natural deciduous forest cover of the PotVeg scenario leads to fewer excursions into the upper left hot/dry portion of the ($\lambda q, c_p t$) phase-space (Figure 4b), indicating that natural deciduous forests modulate the instances of extremely hot, dry summertime conditions in Iowa, relative to the crop-covered historical land use scenario (Figure 4a). Figures 4a and b also demonstrate that in most years the mean July diurnal cycle of temperature and humidity is much more tightly constrained over forests than over croplands. These results are consistent with Teuling et al. (2010) who found that conservative water use by forests mitigates the impact of the most extreme heatwave events in Europe.

To quantify the frequency and extent of this tempering of hot, dry extremes, we wish to compare how the data from each experiment occupy the most arid (upper left) portion of the mixing diagrams in Figure 4. We calculate the 10^{th} and 90^{th} percentile threshold values for the monthly mean moist enthalpy and aridity, as described in Methods. These threshold values are shown in Figure 4c with solid green (PotVeg) and black (AllHist) lines.

Figure 4c shows that about half of the July values in the AllHist run exceed the 10^{th} percentile threshold for hot, dry conditions determined from the PotVeg run: what is a once-in-a-decade hot, dry summer in the PotVeg scenario is an every-other-year event in the AllHist scenario at this grid point. Figure 5a underscores that this shift in hot, dry summer return interval is not limited to Iowa, and is not limited to July: conversion of forests to cropland has contributed to much of the upper central US and central Europe experiencing extreme hot, dry summers every 2-3 years instead of every 10 years. This signal even stands out in the seasonal zonal mean, with an average doubling of the frequency of these extreme hot, dry summers at 50˚N (Figure 5c). The Wilcoxon rank-sum test used in Figure 5 is conservative, in that the significance test for each pixel is based on differences in the mean only. It thus does not capture pixels with

[1] Nighttime super-saturation in Figure 4b results from extrapolation from the lowest model level down to 2m during post-processing. All results presented here are consistent with calculations performed with mean values from the lowest model level or from 925 mb (not shown), but diurnal cycles were only saved for 2m values.

differences in the distribution tails but no mean value change - a behavior that can arise as a result of land-atmosphere feedbacks (Berg et al. 2014).

While the results presented here emphasize monthly means, we have similarly analyzed the mean afternoon conditions (3-6 pm, red points in Figure 4; 3-6 pm typically captures the maximum temperature and includes the sometimes dramatic afternoon drying which often occurs after the time of peak temperature) as well as the maximum daily temperature and the associated humidity. We find comparable results, with prolonged periods of extreme hot, dry afternoon conditions occurring every 2-3 summers instead of every 10^{th} summer as a result of anthropogenic conversion from mid-latitude forests to crops and pastures (not shown). Some of this similarity stems from the use of monthly mean diurnal cycles rather than values from hourly data—a limitation imposed by data availability. Although the magnitude of the change of extreme occurrence return period is likely to depend on both the model analyzed and assumptions about LULCC history, the size of the shifts we find for GFDL ESM2G points to a non-negligible role for LULCC in shaping the distribution of regional extremes in the current climate.

3.2 Tropical response to historical LULCC

Tropical regions with intensive crop development (India, the Sahel, SE Asia; Figure 1) show an LAI decrease, as in the mid-latitudes (Figure 2). However, LAI increases in three tropical broadleaf forest regions: (1) the Amazon, with ~10% pasture around the margin of the forest region and ~10% secondary throughout; (2) central Africa, with a strong imprint of secondary vegetation; and (3) the northeast margin of Australia, with about 50% replacement by pasture and ~10% secondary. Under the LULCC scenario assumptions in the Hurtt et al. (2011) reconstruction, 6.7% of croplands and pastures are abandoned annually (i.e., converted to secondary) and an equal area of new croplands and pastures are created by conversion of natural or secondary lands. Previous studies have highlighted the importance of secondary vegetation and indicated that shifting cultivation practices in tropical regions play an important role in carbon dynamics (Shevliakova et al., 2009; Houghton et al., 2012). Because of their effect on vegetation characteristics, such practices could also modulate biophysical feedbacks.

In the mean, AllHist is more humid in much of Amazon and Australia in austral summer (Figure 3). Figure 4d shows the shift towards higher humidity and correspondingly higher moist enthalpy for December conditions at a single grid point in the semi-arid Nordeste region of Brazil, while Figure 5 shows that this is a year-round signal throughout the tropics. Each of the tropical land regions shows a two-to-three-fold increase in the frequency of high humidity events in all seasons (Figure 5b-c). This tropics-wide temperature and humidity response (Figure 3) is likely linked to the increased GPP throughout the tropics (Figure 2d). Studies focusing on only the temperature effect of LULCC may not capture the significant humidity-driven changes in near-surface tropical climate highlighted here. Given the physiological importance of moist enthalpy (or similarly wet bulb temperature) for humans and mammals (Sherwood and Huber, 2010) and

the rapid rise in urbanization in tropical regions, this highlights the importance of LULCC as a necessary component in any characterization of future climate conditions and heat stress in tropical regions.

4 Conclusions

This study lends a new perspective on the role of anthropogenic LULCC on regional climate extremes, both through the novel consideration of the joint temperature–humidity response to historical LULCC and through the use of an ESM which accounts for the critical processes of wood harvesting, shifting cultivation, and secondary vegetation growth. Within GFDL EMS2G, the inclusion of anthropogenic LULCC produces a two-to-four-fold increase in the frequency of hot, dry summers in much of the mid-latitudes, as well as a two-to-four-fold increase of high humidity conditions throughout the tropics during all seasons, compared to what is seen with potential vegetation. The mid-latitude response is consistent with earlier assessments of changes in summertime mean temperatures in response to historical LULCC (e.g., Findell et al., 2007, 2009), but here we show that these changes in mean temperatures extend to changes in extremes of temperature and humidity. Given the importance of both of these variables for the health and well-being of humans and ecosystems, this bivariate approach enhances our ability to understand the broader impact of LULCC. The tropical response hinges on the inclusion of secondary forest growth, wood harvesting, and shifting cultivation in ESM2G—processes not included in all land models. Shevliakova et al. (2009) and Houghton et al. (2012) showed that these practices impact carbon dynamics; here we demonstrate that they also impact the tropical hydrologic cycle. These substantial and significant impacts call attention to the critical need to include land use-related processes in future projections of climate.

References

Alkama, R., and A. Cescatti, 2016. Biophysical climate impacts of recent changes in global forest cover. *Science, 351,* Issue 6273, pp 600-604.

Berg, A. M., B. R. Lintner, K. L. Findell, S. Malyshev, P. C. Loikith, and P. Gentine, 2014: Impact of soil moisture-atmosphere interactions on surface temperature distribution**.** *Journal of Climate, 27***,** DOI:10.1175/JCLI-D-13-00591.1 .

Berg, A. M., and co-authors, 2016: Land-atmosphere feedbacks amplify aridity increase over land under global warming. *Nature Climate Change*, doi:10.1038/nclimate3029.

Betts, A.K., 1992: FIFE atmospheric boundary layer budget methods. *J. Geophys. Res., 97*, 18 523–18 531.

Bonan, G.B., 1999: Frost followed the plow: impacts of deforestation on the climate of the United States. *Ecological Applications, 9,* 1305-1315.

Chen, L. and P. Dirmeyer, 2016: Adapting observationally based metrics of biogeophysical feedbacks from land cover/land use change to climate modeling. *Environ. Res. Lett., 11.* doi:10.1088/1748-9326/11/3/034002.

Christidis, N., P. A. Stott, G. C. Hegerl, and R. A. Betts, 2013: The role of land use change in the recent warming of daily extreme temperatures. *Geophys. Res. Lett., 40,* 589–594, doi:10.1002/grl.50159.

Davin, E.L., S.I. Seneviratne, P. Ciais, A. Olioso, and T. Wang, 2014. Preferential cooling of hot extremes from cropland albedo management. Proc. Nat. Acad. Sci., doi:/10.1073/pnas.1317323111.

De Noblet-Ducoudre, N. and co-authors, 2012. Determining Robust Impacts of Land-Use-Induced Land Cover Changes on Surface Climate over North America and Eurasia: Results from the First Set of LUCID Experiments. *J. Clim.*, 25, 3261-3281.

Dunne, J. P., and co-authors, 2012: GFDL's ESM2 global coupled climate-carbon Earth System Models Part I: Physical formulation and baseline simulation characteristics**.** *Journal of Climate, 25,* DOI:10.1175/JCLI-D-11-00560.1.

Dunne, J. P., and co-authors, 2013: GFDL's ESM2 global coupled climate-carbon Earth System Models Part II: Carbon system formulation and baseline simulation characteristics**.** *Journal of Climate, 27,* DOI:10.1175/JCLI-D-12-00150.1.

Findell, K. L., T. R. Knutson, and P. C. D. Milly, 2006: Weak simulated extratropical responses to complete tropical deforestation. *Journal of Climate, 19,* 2835-2850.

Findell, K.L, E. Shevliakova, P.C.D. Milly, and R.J. Stouffer, 2007: Modeled Impact of Anthropogenic Land Cover Change on Climate. *J. Clim., 20,* 3621-3634, doi:10.1175/JCLI4185.1.

Findell, K. L., A..J. Pitman, M. H. England, and P. J. Pegion, 2009: Regional and global impacts of land cover change and sea surface temperature anomalies**.** *Journal of Climate, 22,* DOI:10.1175/2008JCLI2580.1.

Fischer, E.M., and C. Schär, 2010: Consistent geographical patterns of changes in high-impact European heatwaves. *Nature Geoscience, 3,* 398-403, doi:10.1038/NGEO866.

Houghton, R.A. and co-authors, 2012. Carbon emissions from land use and land-cover change. *Biogeosciences*, 9, 5125-5142, doi:10.5194/bg-9-5125-2012.

Hurtt, G. C., and co-authors, 2011: Harmonization of land-use scenarios for the period 1500–2100: 600 years of global gridded annual land-use transitions, wood harvest, and resulting secondary lands. *Climatic Change, 109*, 117–161, doi:10.1007/s10584-011-0153-2.

Jackson, R.B., and co-authors, 2005: Trading water for carbon with biological carbon sequestration. *Science, 310,* 1944-1947.

Khanna, J., and D. Medvigy, 2014: Strong control of surface roughness variations on the simulated dry season regional atmospheric response to contemporary deforestation in Rondônia, Brazil. *Journal of Geophysical Research: Atmospheres, 119,* 13,067-13,078.

Knutson, T. R., and J. J. Ploshay, 2016: Detection of anthropogenic influence on a summertime heat stress index**.** *Climatic Change, 138***,** DOI:10.1007/s10584-016-1708-z .

Lawrence, D. M., and co-authors, 2016: The Land Use Model Intercomparison Project (LUMIP) contribution to CMIP6: rationale and experimental design. *Geosci. Model Dev., 9,* 2973-2998, doi:10.5194/gmd-9-2973-2016.

Lemordant, L., P. Gentine, M. Stéfanon, P. Drobinski, and S. Fatichi, 2016: Modification of land-atmosphere interactions by CO_2 effects: Implications for summer dryness and heat wave amplitude, *Geophys. Res. Lett., 43*, doi:10.1002/2016GL069896.

Lee, X., and co-authors, 2011: Observed increase in local cooling effect of deforestation at higher latitudes. *Nature, 479,* 384-387, doi:10.1038/nature10588.

Li, Y., M. Zhao, S. Motesharrei, Q. Mu, E. Kalnay, and S. Li, 2015: Local cooling and warming effects of forests based on satellite observations." *Nature Communications, 6,* doi:10.1038/ncomms7603.

Malyshev, S., E. Shevliakova, R.J. Stouffer, and S.W. Pacala, 2015: Contrasting Local versus Regional Effects of Land-Use-Change-Induced Heterogeneity on Historical Climate: Analysis with the GFDL Earth System Model. *J. Clim.*, 28, 5448-5469.

Milly, P. C. D., and co-authors, 2014: "An enhanced model of land water and energy for global hydrologic and earth-system studies**."** *Journal of Hydrometeorology, 15,* DOI:10.1175/JHM-D-13-0162.1.

Miralles, D.G., A.J. Teuling, C.C. van Heerwaarden, and J. Vilà-Guerau de Arellano, 2014: Mega-heatwave temperatures due to combined soil desiccation and atmospheric heat accumulation. *Nature Geoscience, 7*, 345-349.

Oleson, K.W., Bonan, G.B., Levis, S. et al. Climate Dynamics (2004) 23: 117. doi:10.1007/s00382-004-0426-9

Pal, J.S. and E.A.B. Elthair, 2016: Future temperature in southwest Asia projected to exceed a threshold for human adaptability. *Nature Climate Change, 6*, 197–200, doi:10.1038/nclimate2833.

Pitman, A.J., and co-authors, 2009: Uncertainties in climate responses to past land cover change: First results from the LUCID intercomparison study. *Geophys. Res. Lett., 36,* L14814, doi:10.1029/2009GL039076.

Pitman, A.J., and co-authors, 2012: Effects of land cover change on temperature and rainfall extremes in multi-model ensemble simulations. *Earth Syst. Dynam. 3,* 213-231. doi:10.5194/esd-3-213-2012.

Santanello, J.A., C.D. Peters-Lidard, S. V. Kumar, C. Alonge, and W.-K. Tao, 2009: A modeling and observational framework for diagnosing local land–atmosphere coupling on diurnal time scales. *J. Hydrometeor., 10*, 577–599.

Sherwood, S.C. and M. Huber, 2010: An adaptability limit to climate change due to heat stress. *Proc. Nat. Acad. Sci., 107*, doi:10.1073/pnas.0913352107.

Shevliakova, E., and co-authors, 2009: Carbon cycling under 300 years of land use change: Importance of the secondary vegetation sink. *Global Biogeochemical Cycles, 23,* GB2022, doi:10.1029/2007GB003176.

Shevliakova , E., R.J. Stouffer, S. Malyshev, J.P. Krasting, G.C. Hurtt, and S.W. Pacala, 2013: Historical warming reduced due to enhanced land carbon uptake. *Proc. National Academy of Sciences, 110,* 16730-16735.

Stefanon, M., P. Drobinski, F. D'Andrea, and N. de Noblet-Ducoudré, 2012: Effects of interactive vegetation phenology on the 2003 summer heat waves. *J. Geophys. Res., 117,* D24103, doi:10.1029/2012JD018187.

Strack, J.E., R.A. Pielke Sr., L.T. Steyaert, and R.G. Knox, 2008: Sensitivitiy of June near-surface temperatures and precipitation in the eastern United States to historical land cover changes since European settlement. *Water Resources Research, 44*, W11401, doi:10.1029/2007WR006546.

Stott, P.A., D.A. Stone, and M.R. Allen, 2004: Human contributions to the European heatwave of 2003. *Nature, 432*, 610-614, doi:10.1038/nature03089.

Taylor K. E., R. J. Stouffer, and G. A. Meehl, 2012: An overview of CMIP5 and the experiment design. *Bulletin of the American Meteorological Society, 93*, 485-498, doi:10.1175/bams-d-11-00094.1.

Teuling, A. J., and co-authors, 2010: Contrasting response of European forest and grassland energy exchange to heatwaves, *Nat. Geosci., 3*, 722–727.

Van Heerwarden, C.C. and A.J. Teuling, 2014: Disentangling the response of forest and grassland energy exchange to heatwaves under idealized land–atmosphere coupling. *Biogeosciences, 11*, 6159–6171, doi:10.5194/bg-11-6159-2014

von Storch, H., and F. W. Zwiers, 1999: *Statistical Analysis in Climate Research*. Cambridge University Press, 484 pp.

Wickham, J. D., T. G. Wade, and K. H. Riitters, 2012: Comparison of cropland and forest surface temperatures across the conterminous United States. *Agricultural and Forest Meterology, 166-7*, 137-143.

Acknowledgements

The authors would like to thank Chris Milly and Tom Knutson for providing helpful comments on the manuscript.

Author contributions

KLF designed the study, analyzed the model output, and wrote the paper. JPK ran the simulations. ES and SM provided important insight on aspects of the land and vegetation model. JAS provided important insight on the use of mixing diagrams. AB, BRL, and PG contributed to the study design and analysis of results. All authors contributed to the writing and revising of the manuscript.

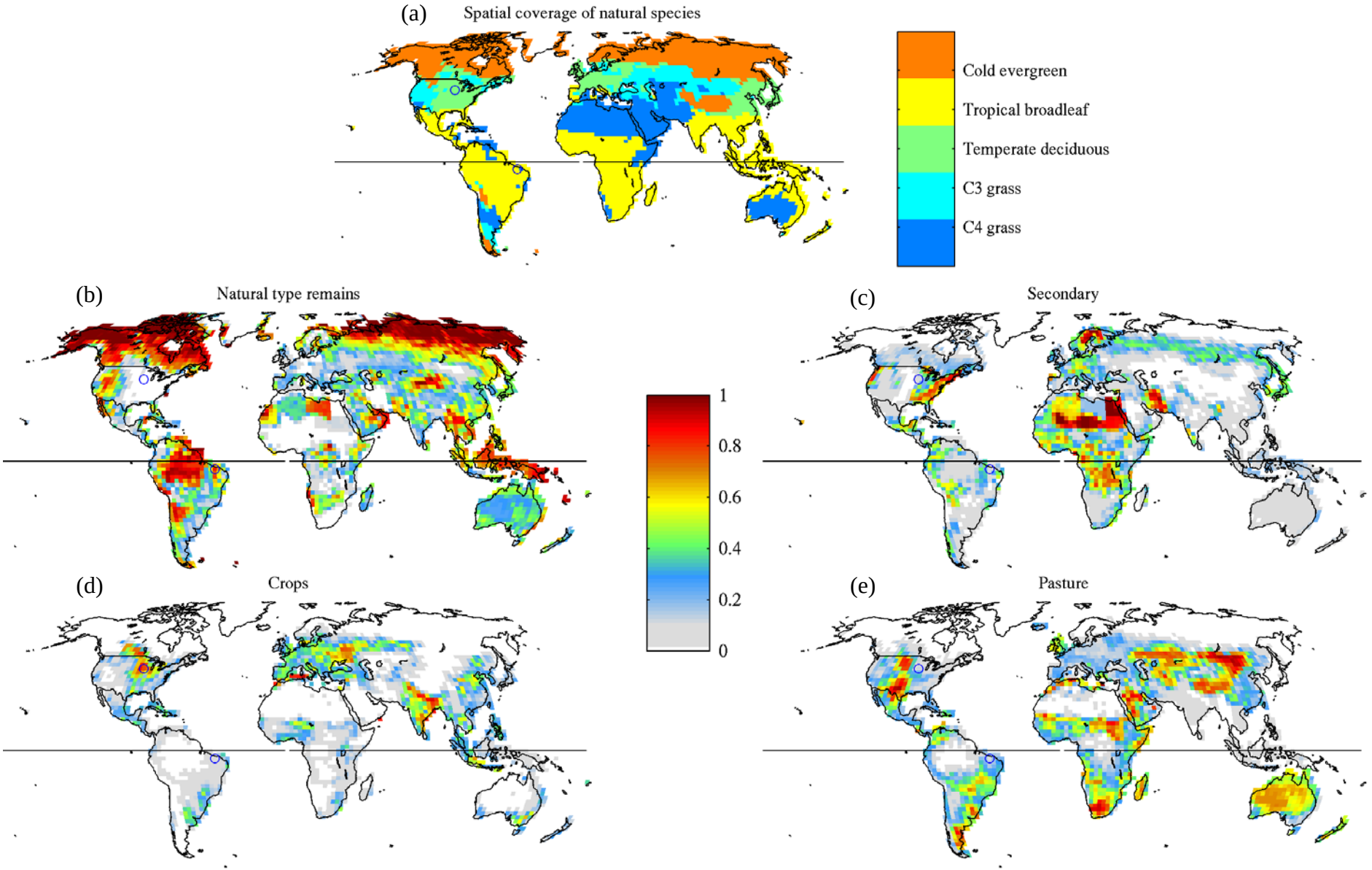

Figure 1: (a) Natural vegetation types. Percent of land remaining as (b) natural type, or converted to (c) secondary, (d) crops, and (e) pasture. (b-e) Averaged over 1981-2005 in two ensemble members of the AllHist simulations. Blue circles over points in the central United States and Eastern Brazil show locations of data used in Figure 4.

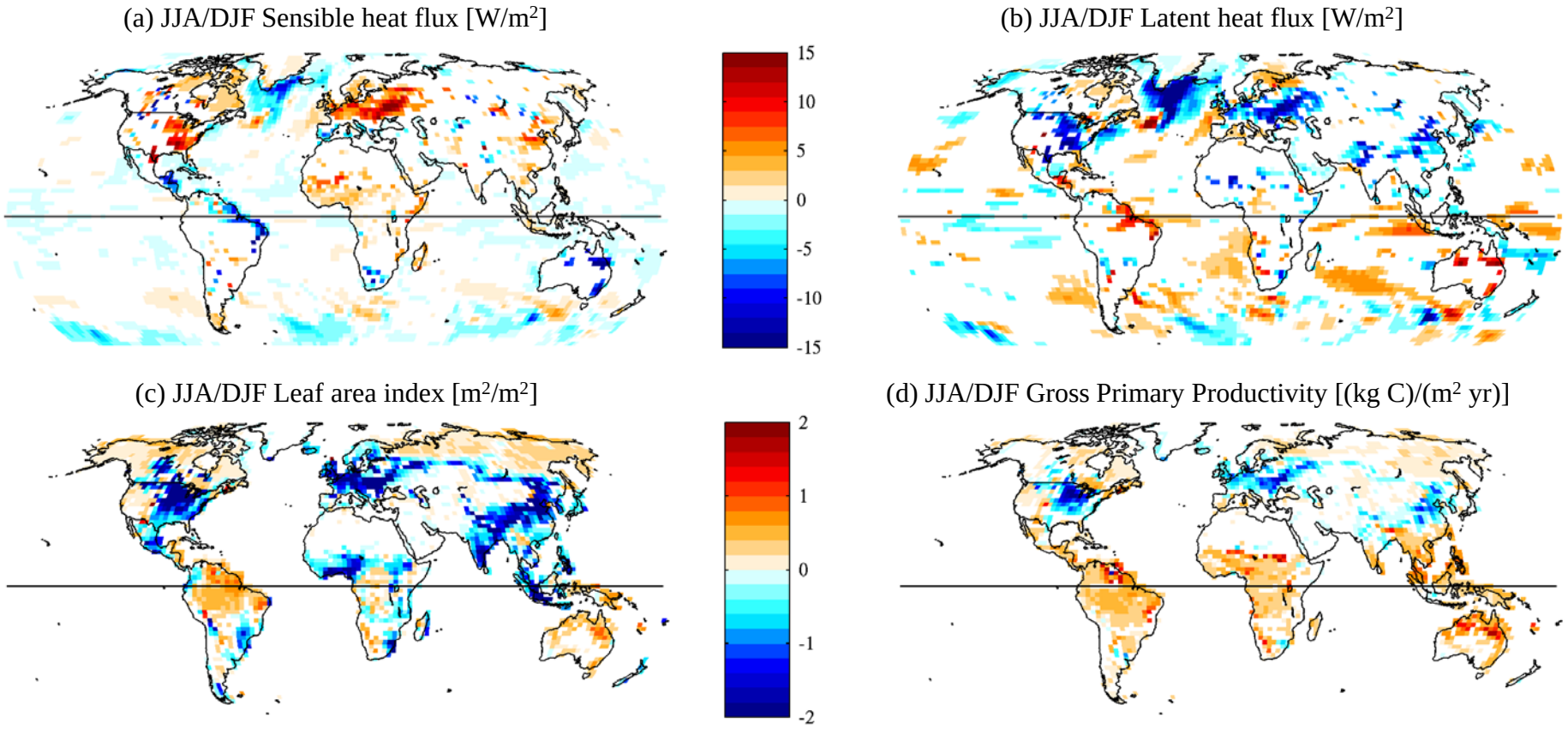

Figure 2: Mean differences between the AllHist and the PotVeg simulations for June-August in the northern hemisphere and for December-February for the southern hemisphere, averaged over the years 1981-2005. (a) Sensible heat flux; (b) latent heat flux; (c) LAI; and (d) gross primary productivity. Differences shown pass a standard t-test at the 90% significance level.

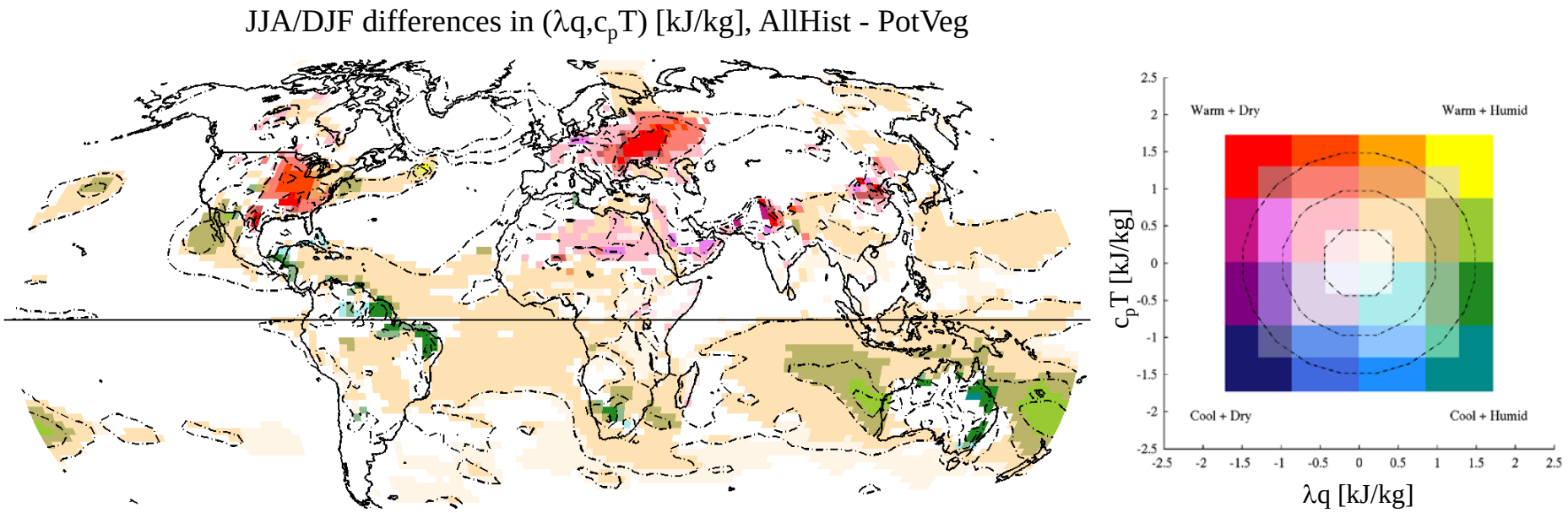

Figure 3: Mean differences (AllHist – PotVeg) for June-August in the northern hemisphere and for December-February for the southern hemisphere in (λq, $c_p T$) phase space, with differences of 2m values of λq and $c_p T$ plotted according to the 2-dimensional colorgrid. q is specific humidity, λ is the latent heat of condensation, T is temperature, and c_p is the specific heat of dry air at constant pressure. Colors reflect the vector differences of the means when plotted on conserved variable diagrams like those shown in Figure 4. Differences shown have at least one of the two variables passing a modified t-test at the 90% significance level. Contours every 0.5 kJ/kg.

Figure 4: (a-b) For a single grid point in Central Iowa (location indicated on Figure 1), AllHist (a) and PotVeg (b) runs, 2 ensemble members each, 1981-2005 (50 years total), 7 am – 6 am, mean monthly diurnal cycles of 2m values of λq and c_pT for July plotted in conserved-variable space typically used for mixing diagrams. Red symbols for 3 – 6 pm values. (c) Thick lines: mean diurnal cycles from (a) and (b); red lines from 3 – 6 pm; plus signs: mean (λq,c_pT) for each of the 50 years. (d) As in (c), but for a grid cell in East Brazil for December. In all plots, dashed black lines: constant relative humidity; dashed red lines: constant moist enthalpy (ME). In (c) and (d), solid lines are thresholds for the top 10th percentile monthly mean values of ME and the aridity measure perpendicular to ME. In all plots, green is used for the PotVeg runs, black for the AllHist runs.

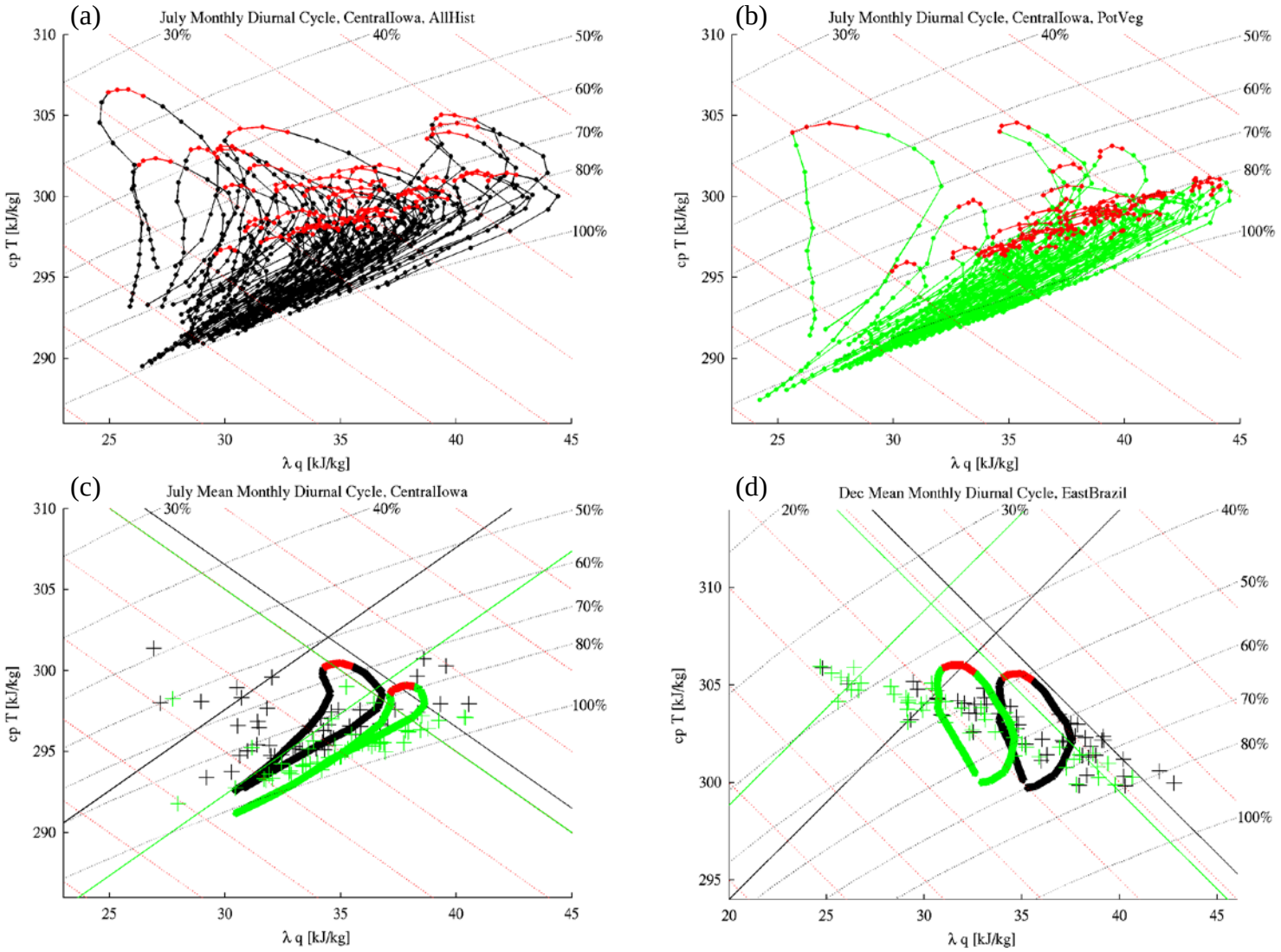

Figure 5: Impact of LULC changes on extremes. AllHist return periods for exceedance of once-in-a-decade event thresholds determined from the PotVeg run for (a) the aridity threshold in June, (b) the moist enthalpy threshold in December, and (c) seasonal, latitudinal means for aridity thresholds (dashed lines) and moist enthalpy thresholds (solid lines). In (a) and (b), colors are only shown where the medians of the 50-year samples are significantly different according to a Wilcoxon rank sum test at the 5% level. In (c) grey vertical lines are drawn at 6, 10, and 14-year return periods (5±2 exceedances in 50 years), with 10 years representing the null hypothesis (no change from PotVeg). In the mid-latitudes, summertime aridity exceeds these bounds over a ~25 degree latitude band. This persists into autumn in the central ~10 degrees. In the tropics, all seasons demonstrate more frequent high moist enthalpy conditions.

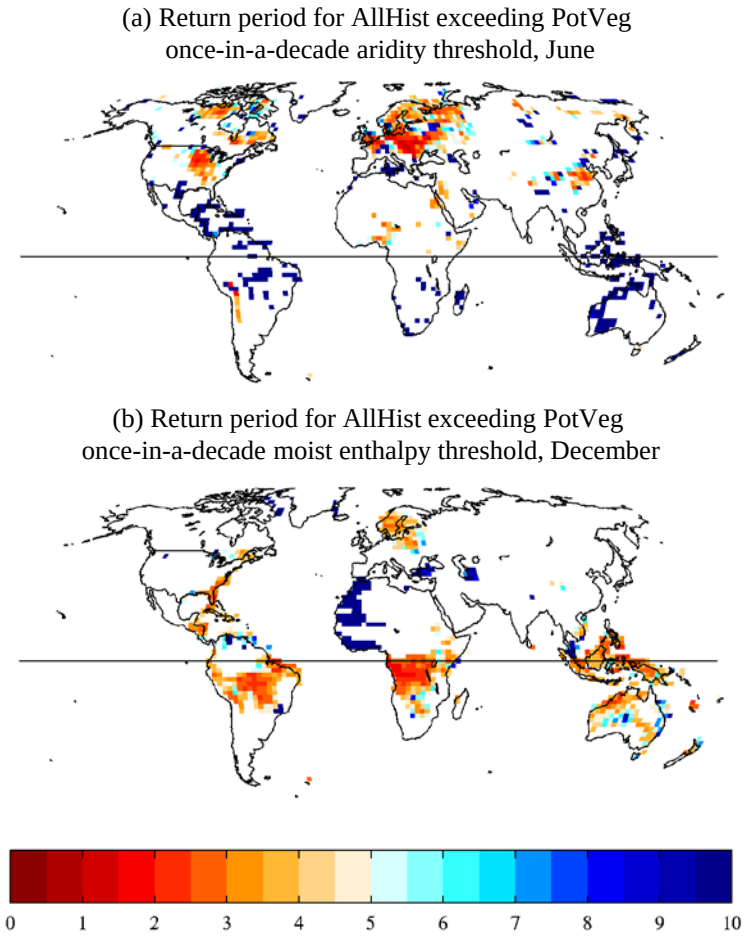

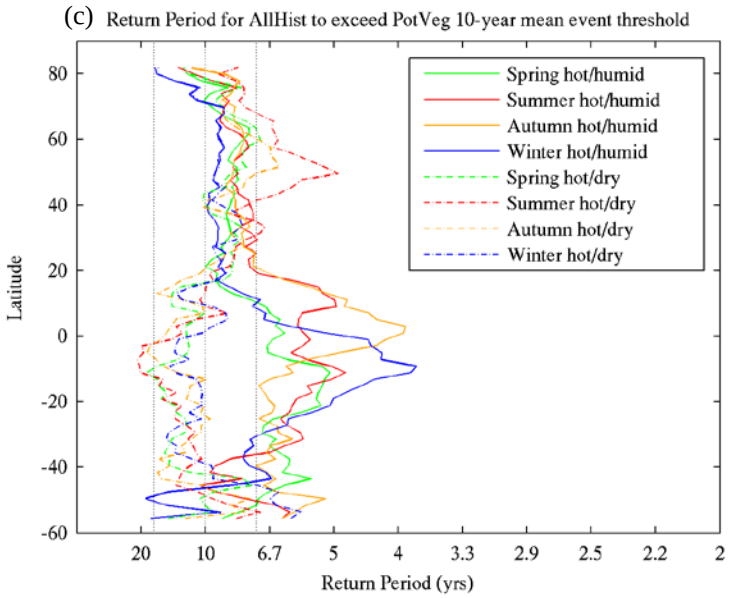

Supplemental figures

Figure S1. (a) Like Figure 5a, but for relative humidity. (b) Like Figure 5b, but for wet-bulb temperature.